Nanocrystalline lanthanide-doped $Lu_3Ga_5O_{12}$ garnets: interesting materials for light-emitting devices

2010 Nanotechnology 21 175703

(http://iopscience.iop.org/0957-4484/21/17/175703)

Nanotechnology **21** (2010) 175703 (12pp) doi:10.1088/0957-4484/21/17/175703

Nanocrystalline lanthanide-doped $Lu_3Ga_5O_{12}$ garnets: interesting materials for light-emitting devices

V Venkatramu[1], M Giarola[2], G Mariotto[2], S Enzo[3], S Polizzi[4], C K Jayasankar[5], F Piccinelli[6], M Bettinelli[6] and A Speghini[6]

[1] Department of Physics, Yogi Vemana University, Kadapa 516 003, India
[2] Dipartimento di Informatica, Università di Verona, Strada Le Grazie 15, I-37134 Verona, Italy
[3] Dipartimento di Chimica, Università di Sassari and INSTM, UdR Sassari, Via Vienna 2, I-07100 Sassari, Italy
[4] Dipartimento di Chimica Fisica, Università di Venezia and INSTM, UdR Venezia, Via Torino 155/b, I-30172 Venezia—Mestre, Italy
[5] Department of Physics, Sri Venkateswara University, Tirupati 517 502, India
[6] Laboratorio di Chimica dello Stato Solido, DB, Università di Verona and INSTM, UdR Verona, Ca' Vignal, Strada Le Grazie 15, I-37134 Verona, Italy

E-mail: adolfo.speghini@univr.it

Received 13 January 2010, in final form 5 March 2010
Published 6 April 2010
Online at stacks.iop.org/Nano/21/175703

Abstract

Nanocrystalline $Lu_3Ga_5O_{12}$, with average particle sizes of 40 nm, doped with a wide variety of luminescent trivalent lanthanide ions have been prepared using a sol–gel technique. The structural and morphological properties of the powders have been investigated by x-ray powder diffraction, high resolution transmission electron microscopy and Raman spectroscopy. Structural data have been refined and are presented for Pr^{3+}, Eu^{3+}, Gd^{3+}, Ho^{3+}, Er^{3+} and Tm^{3+} dopants, while room temperature excited luminescence spectra and emission decay curves of Eu^{3+}-, Tm^{3+}- and Ho^{3+}-doped $Lu_3Ga_5O_{12}$ nanocrystals have been measured and are discussed. The Eu^{3+} emission spectrum shows typical bands due to $^5D_0 \rightarrow {}^7F_J$ ($J = 0, 1, 2, 3, 4$) transitions and the broadening of these emission bands with the non-exponential behaviour of the decay curves indicates the presence of structural disorder around the lanthanide ions. Lanthanide-doped nanocrystalline $Lu_3Ga_5O_{12}$ materials show better luminescence intensities compared to Y_2O_3, $Gd_3Ga_5O_{12}$ and $Y_3Al_5O_{12}$ nanocrystalline hosts. Moreover, the upconversion emission intensity in the blue-green region for the Tm^{3+}- and Ho^{3+}-doped samples shows a significant increase upon 647.5 nm excitation with respect to other common oxide hosts doped with the same lanthanide ions.

1. Introduction

In the last few years, many efforts have been devoted to the study of lanthanide-doped nanocrystals. It has been found that nanosized materials can maintain excellent spectroscopic properties typical of bulk systems, making them interesting as materials for devices of technological importance, especially in the photonic and bioimaging fields [1–5]. Among oxide-based materials, garnets have gained a considerable degree of attention due to their interesting chemical and physical properties such as high density, high thermal conductivity and hardness, and good chemical stability [6]. Many investigations on the luminescence properties of lanthanide-doped garnets have shown that they can be usefully employed as laser crystals, phosphors and upconverter materials [7–10]. In this class of materials, the luminescence properties of lutetium-based garnets, such as $La_3Lu_2Ga_3O_{12}$ (LLGG), $Lu_3Al_5O_{12}$ (LuAG) or $Lu_3Ga_5O_{12}$ (LuGG) single crystals or transparent ceramics [11–16] doped with lanthanide ions are particularly promising. Specifically, Ce^{3+}-or Yb^{3+}-doped lutetium-based garnets have recently gained much attention as materials for scintillator detectors, especially for medical

diagnostic imaging using gamma-rays or x-rays [17, 18]. Interestingly, theoretical investigations on ten Er^{3+}-doped garnets clearly indicate that the upconversion properties can be enhanced for the LuGG host with respect to the more popular YAG host [19]. Moreover, recent studies have described the luminescence of rare-earth-doped lutetium-based compounds, because of their excellent emission properties [20]. Some efforts have been spent in the recent past also to investigate the emission properties of rare-earth-doped nanocrystalline garnets [21], in particular $Y_3Al_5O_{12}$ (YAG) [22, 23] and $Gd_3Ga_5O_{12}$ (GGG) [6, 24]. On the other hand, only a few papers have been published on the morphological and luminescence properties of lanthanide-doped nanocrystalline LuGG powders [25, 26]. For these reasons we found it interesting to extend the previous investigations by considering this promising host in nanocrystalline form when doped with lanthanide ions. Detailed structural and morphological data are reported for Pr^{3+}, Eu^{3+}, Gd^{3+}, Ho^{3+}, Er^{3+} and Tm^{3+} dopants; spectroscopic properties of the nanocrystalline materials have been investigated for Eu^{3+}-, Tm^{3+}- and Ho^{3+}-doped samples, considering in particular the upconversion properties for Tm^{3+}- and Ho^{3+}-doped samples. The spectroscopic properties have been compared with those observed for other oxide nanocrystalline hosts. Lanthanide-doped nanocrystalline LuGG powders have been prepared using a sol–gel technique employing citric acid as a chelating ligand and polyethylene glycol (PEG) as a cross-linking agent. This method is, in fact, particularly easy, useful and friendly from an environmental point of view because the starting reagents are non-toxic and relatively low processing temperatures are employed with respect to other techniques.

2. Experimental details

2.1. Sample preparation

Undoped $Lu_3Ga_5O_{12}$ and lanthanide-doped $Lu_{2.97}Ln_{0.03}Ga_5O_{12}$ (Ln = Pr, Eu, Gd, Ho, Er or Tm) nanocrystalline samples were prepared using a sol–gel synthesis. The starting reagents were $Ga(NO_3)_3{\cdot}6H_2O$ (Aldrich, 99.999%), $Lu(NO_3)_3{\cdot}5H_2O$ (Aldrich, 99.999%), $Pr(NO_3)_3{\cdot}5H_2O$ (Aldrich, 99.9%), $Eu(NO_3)_3{\cdot}5H_2O$ (Aldrich, 99.9%), $Gd(NO_3)_3{\cdot}5H_2O$ (Aldrich, 99.9%), $Ho(NO_3)_3{\cdot}5H_2O$ (Aldrich, 99.9%), $Er(NO_3)_3{\cdot}5H_2O$ (Aldrich, 99.9%), $Tm(NO_3)_3{\cdot}5H_2O$ (Aldrich, 99.9%), citric acid (Fluka, 99.5%) and polyethylene glycol (PEG) (Spectra Tech. Inc.). Stoichiometric quantities of the metal nitrates were dissolved in 25 ml of a 1 M nitric acid aqueous solution under stirring. A suitable quantity of citric acid, corresponding to a 2:1 molar ratio amount with respect to the metal nitrates, was added and dissolved in the solution under stirring and heating (80 °C). Then, a quantity of PEG corresponding to three times the mass amount of citric acid was added to the solution. The solution was stirred for 2 h and then dried at 90 °C for 36 h. The obtained gel was fired at 500 °C for 2 h in order to remove the residual nitrates and organics. Finally, the powder sample was annealed at 900 °C for 16 h in air. Hereafter, the prepared samples are referred as LuGG:Ln (Ln = Pr, Eu, Gd, Tm, Ho, Er). All the samples contain 1 mol% of the lanthanide ion with respect to Lu^{3+}.

2.2. X-ray powder diffraction

The x-ray powder diffraction (XRPD) patterns for the nanocrystalline samples were recorded overnight with a Bruker D8 diffractometer in the Bragg–Brentano geometry using Cu Kα radiation (λ = 1.5418 Å). The x-ray generator worked at a voltage of 40 kV and a current of 40 mA and the goniometer was equipped with a graphite monochromator in the diffracted beam. The resolution of the instrument (divergent and antiscatter slits of 0.5°) was determined using α-SiO_2 and α-Al_2O_3 powder standards which are supposed to be free from lattice defects and with sufficiently large average grain size to minimize any sample broadening. The powder patterns were analysed according to the Rietveld method [27] using the program MAUD [28] running on a personal computer. It is worth recalling that the MAUD program takes into account precisely the instrument broadening resolution and, under the selected assumption of isotropic peak broadening as a function of reciprocal space, performs the separation of the lattice strain contribution from the broadening originating from the reduced crystallite size. Relative agreement factors R_{wp} and R_B are generally reported to determine the ability of the implemented structural model to account for the experimental data, which are unavoidably affected by statistical noise due to the limited time of pattern collection.

2.3. Transmission electron microscopy (TEM)

TEM and high resolution TEM (HRTEM) images were taken with a JEOL 3010 high resolution electron microscope (1.7 nm point-to-point), operating at 300 kV, equipped with a Gatan slow-scan CCD camera (Model 794) and an Oxford Instrument EDS microanalysis detector (Model 6636). The powder was dispersed in an isopropyl alcohol solution and deposited on a holey carbon film.

2.4. Raman spectroscopy

Vibrational properties of undoped nanocrystalline $Lu_3Ga_5O_{12}$ powders were probed by micro-Raman spectroscopy. To this aim the Raman spectrum was excited at room temperature using the blue line at 488.0 nm of an Ar^+/Kr^+ mixed-gas ion laser and were detected by a CCD, with 1024 pixels × 256 pixels, cryogenically cooled by liquid nitrogen. The laser beam was focused onto the sample surface, with a spot size of about 2 μm, by a 100× objective with NA = 0.9. The Stokes component of the backscattered radiation was analysed by a triple-monochromator spectrometer (Horiba Jobin Yvon, model T64000), set in double-subtractive/single configuration, and equipped with 1800 grooves mm^{-1} gratings, which ensured a spectral resolution better than 1 cm^{-1}/pixel over the scanned spectral range. In order to check the origin of the observed spectral bands (i.e. to discriminate between scattering and emission processes) the laser line at 514.5 nm was usefully exploited for the spectra excitation.

2.5. Infrared reflectance spectroscopy

Room temperature diffuse reflectance spectra in the mid-infrared region (MIR) were measured at room temperature

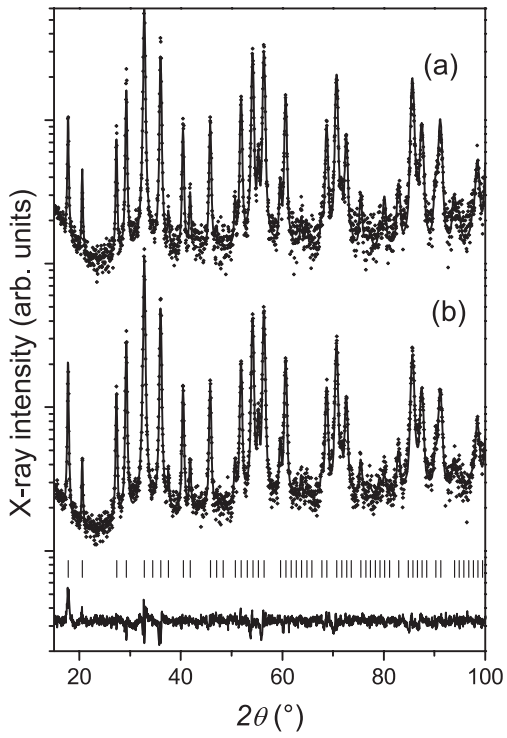

Figure 1. X-ray diffraction patterns of europium- (a) and erbium (b)-doped nanocrystalline LuGG. Dots: experimental data; solid lines: Rietveld fits. The bar sequence marks the expected position of each peak according to the lattice parameter value.

using a Nicolet Magna 760 FTIR spectrometer using an aluminized mirror as a reference.

2.6. Luminescence spectra and decay curves

The emission spectra of Tm^{3+}- and Ho^{3+}-doped LuGG samples were measured using the above-mentioned set-up for the collection of Raman spectra. Moreover, a tunable dye laser (Quanta System) operating with Exalite 395, pumped by the third harmonic (355 nm) of the fundamental radiation of a Quanta System pulsed Nd:YAG laser, was used to measure the emission spectra and emission decay curves for the Eu^{3+}-doped LuGG sample.

For the measurements of the emission decay curves for Ho^{3+}- and Tm^{3+}-doped LuGG nanocrystalline samples, the second harmonic (at 532 nm) of the fundamental radiation of the above-mentioned pulsed Nd:YAG laser was employed as the excitation source. The emission radiation was collected using an optical fibre and dispersed with a Jobin Yvon HR460 half-metre monochromator equipped with a 1200 lines mm^{-1} grating. The decay curves were measured with a Hamamatsu GaAs photomultiplier connected to a Le Croy Waverunner 500 MHz digital oscilloscope.

3. Results and discussion

3.1. Structural and morphological properties

The XRPD patterns were measured for the Pr^{3+}-, Eu^{3+}-, Gd^{3+}-, Er^{3+}-, Tm^{3+}- and Ho^{3+}-doped nanocrystalline samples. As an example, the patterns for the Eu^{3+}-and Er^{3+}-doped samples and their Rietveld fits, performed with the MAUD software, are shown as solid lines in figure 1, as dotted and solid lines, respectively. The structural and microstructural parameters obtained at the end of the fit are reported in table 1. On the basis of these results it can be inferred that the samples under investigation, with nominal stoichiometry Lu/Ga = 3/5, are cubic garnet single phases, with space group $Ia\bar{3}d$ (O_h^{10}). The $Lu_3Ga_5O_{12}$ garnet has a lattice parameter of 12.188 Å with eight formula units per unit cell and possesses three crystallographically distinct D_2, S_4 and S_6 cation sites [29]. The Lu^{3+} ions are located in the dodecahedral D_2 sites and the Ga^{3+} ions are located in the S_4 (tetrahedral) and S_6 (octahedral) sites. The lattice parameters for the lanthanide-doped LuGG samples turn out to be slightly larger than the value reported in the literature for LuGG single crystals [29], due to the presence of the doping agents. Analysis of the line broadening using the MAUD software across the various (*hkl*) reflections provides an average crystallite size around 50 nm with a lattice strain density of about 1.5×10^{-3} (see table 1) which can be due to local defects such as inclusion of doping elements. Of course, we cannot reject totally other sources of defects such as dislocations or stacking faults. Also, it is known that the average crystallite size values are correlated with the average lattice strain and that this correlation may be better resolved by collecting as many as possible d_{hkl} peak components. The wide angular range of our patterns try to meet this requirement, together with that for highly precise lattice parameter determination.

Table 1. Lattice parameter, crystallite size, lattice strain and goodness of fit for the LuGG-doped lanthanide nanocrystalline samples.

Sample	Lattice parameter (Å)	Crystallite size (nm)	Lattice strain/ 10^{-3}	R_{wp} (%)
LuGG:Pr	12.2031(2)	53(4)	1.21(4)	14.4
LuGG:Eu	12.2072(3)	50(7)	1.40(4)	12.1
LuGG:Gd	12.1990(3)	67(6)	1.05(2)	12.8
LuGG:Ho	12.1984(2)	51(5)	1.26(4)	13.9
LuGG:Er	12.1970(3)	59(7)	1.08(4)	14.1
LuGG:Tm	12.1966(3)	51(6)	1.26(4)	13.7

Figure 2 shows the behaviour of the garnet lattice parameter *a* as a function of the size of the lanthanide ions [30] involved here as doping agents. As can be seen from figure 2, a substantially linear correlation between the lattice parameter of the doped garnet and the dopant ionic radius is observed, within experimental errors. This behaviour indicates that the lanthanide dopants do enter in the garnet lattice, presumably substituting the Lu^{3+} ion. For the europium-doped sample, we obtained a relatively large lattice parameter (see table 1), which was confirmed by the analysis of other XRPD patterns for different batches, supporting that the result is genuine and cannot be attributed to experimental artefacts. In fact, from figure 2, it can be noted that, for the europium-doped specimen the linear correlation between the lattice parameters and the ion size of trivalent europium ion is not followed. The values of the oxidation number for europium can be 2+ or 3+, as found in many compounds, such as, for instance,

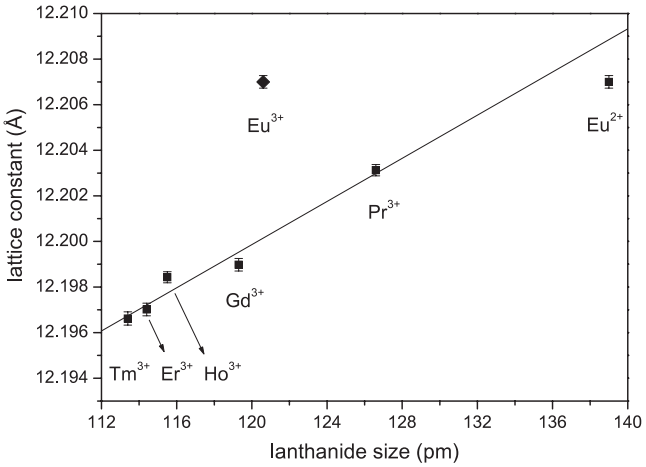

Figure 2. Lattice constant as a function of the dopant ionic radius in eightfold coordination.

Eu_3O_4, while the other lanthanides involved in the present study clearly show a 3+ oxidation state. The presence of Eu^{2+} in the europium-doped sample could explain the observed behaviour, since the ionic radius of Eu^{2+} ion in eightfold coordination is 1.39 Å, a value which is much larger than for Eu^{3+}, 1.206 Å, with the same coordination [30]. Figure 2 shows also that a 2+ oxidation state agrees reasonably well with a linear lattice constant versus ionic size correlation. Therefore, it is reasonable to assume that europium is mainly present in the 2+ oxidation state. An indirect support to this picture is provided by Mihokova *et al* [31], who have observed thermally stimulated luminescence (TSL) from Eu^{3+}-doped LuAG and LuGG nanocrystalline powders, upon x-ray irradiation [31]. In this process, the Eu^{3+} ion tends to trap an electron and therefore an Eu^{2+} ion is formed. Then, the Eu^{2+} ions act as hole traps in a recombination process in which the Eu^{3+} ions are restored. The recombination kinetics for LuGG:Eu nanocrystalline sample is fast at room temperature, with a decay time of a few minutes [31], and for this reason we observed luminescence only from Eu^{3+} ions, as described below. Luminescence measurements under direct x-ray excitation could be very useful to confirm this behaviour.

TEM images for LuGG:Eu nanocrystals show that the sample is made of smooth particles of different shapes and sizes in the range 30–60 nm (see figure 3(a)). Many particles have the shape of interconnected spheres, reminiscent of the original network created in the gel environment (see figure 3(b)). Voids generated during the removal of the organic component can be seen within a large number of particles, occasionally making them hollow spheres (see figure 3(c)). HRTEM images and the electron diffraction pattern confirm the size results of the XRD investigation (see figure 3(d)).

3.2. Vibrational properties

The primitive cell of a garnet lattice contains four formula units (80 atoms) [32]. From a factor group analysis, there are 25 Raman-active phonons which can be classified as 3 A_{1g}, 8 E_g and 14 T_{2g} phonon modes. The observation of only a part of the 25 expected Raman bands seems to be a common feature of the spectra of many garnets, whose band assignments can be summarized as follows [32]. The high frequency modes (800–1100 cm^{-1}) are related to symmetric and asymmetric internal stretching vibrations of rigid GaO_4 tetrahedra, and the modes lying between 450–700 cm^{-1} are assigned to bending motions of these tetrahedra. The remaining lattice modes (150–415 cm^{-1}), involve rotations and translations of the GaO_4 groups, octahedrally coordinated trivalent cations and dodecahedrally coordinated trivalent cations. In an alternative approach, the LuGG garnet structure can be described as a network of GaO_6 octahedra and GaO_4 tetrahedra linked through the corners. These polyhedra are arranged in chains along the three crystallographic directions and form dodecahedral cavities which are occupied by the Lu^{3+} ions. Raman spectra of garnets have also been interpreted on the basis of vibrational modes of the tetrahedral and octahedral units, considering that the vibrations of the different polyhedra are strongly coupled to each other [33–35]. The room temperature Raman spectrum of nanocrystalline LuGG, measured in the 80–900 cm^{-1} Raman shift range, is shown in figure 4. The Raman spectrum presents 13 of the 25 active Raman modes. The observed values of the Raman shifts are very close to those found for a LuGG single crystal at 80 K [33]. The peak energy and the symmetry assignments of the Raman-active modes observed at room temperature in LuGG nanocrystalline powders and those reported by Song *et al* at [33] for a LuGG single crystal are quoted in table 2. According to Saine *et al* [34], the bands comprised in the 580–680 cm^{-1} and 380–460 cm^{-1} ranges can be attributed to the antisymmetric stretching modes of the GaO_4 and GaO_6 polyhedra, respectively. In particular, the strong band observed at 766 cm^{-1} is mostly due to the symmetric stretching mode of the GaO_4 tetrahedron, even if a weaker contribution due to the antisymmetric stretching mode of the same polyhedron could be present [34]. On the other hand, the dominant Raman band at 358 cm^{-1} can be assigned to the symmetric stretching mode of the GaO_4 tetrahedron coupled with a rotational mode

Table 2. Symmetry assignment and energy (cm^{-1}) of active Raman vibrational modes in LuGG single crystal at 80 K [33] and nanocrystalline LuGG at room temperature.

Raman mode symmetry	Raman shift (±3) cm^{-1} Reference [33]	Raman shift (±1) cm^{-1} (present work)
E_g	106	108
T_{2g}	164	166
T_{2g}	178	180
T_{2g}	236	239
E_g	254	258
T_{2g}	268	269
E_g	356	358
T_{2g}	359	
T_{2g}	398	∼400
E_g	436	438
T_{2g}	531	—
A_{1g}	533	538
T_{2g}	603	612
T_{2g}	616	∼625 (sh)
T_{2g}	765	766
A_{1g}	767	

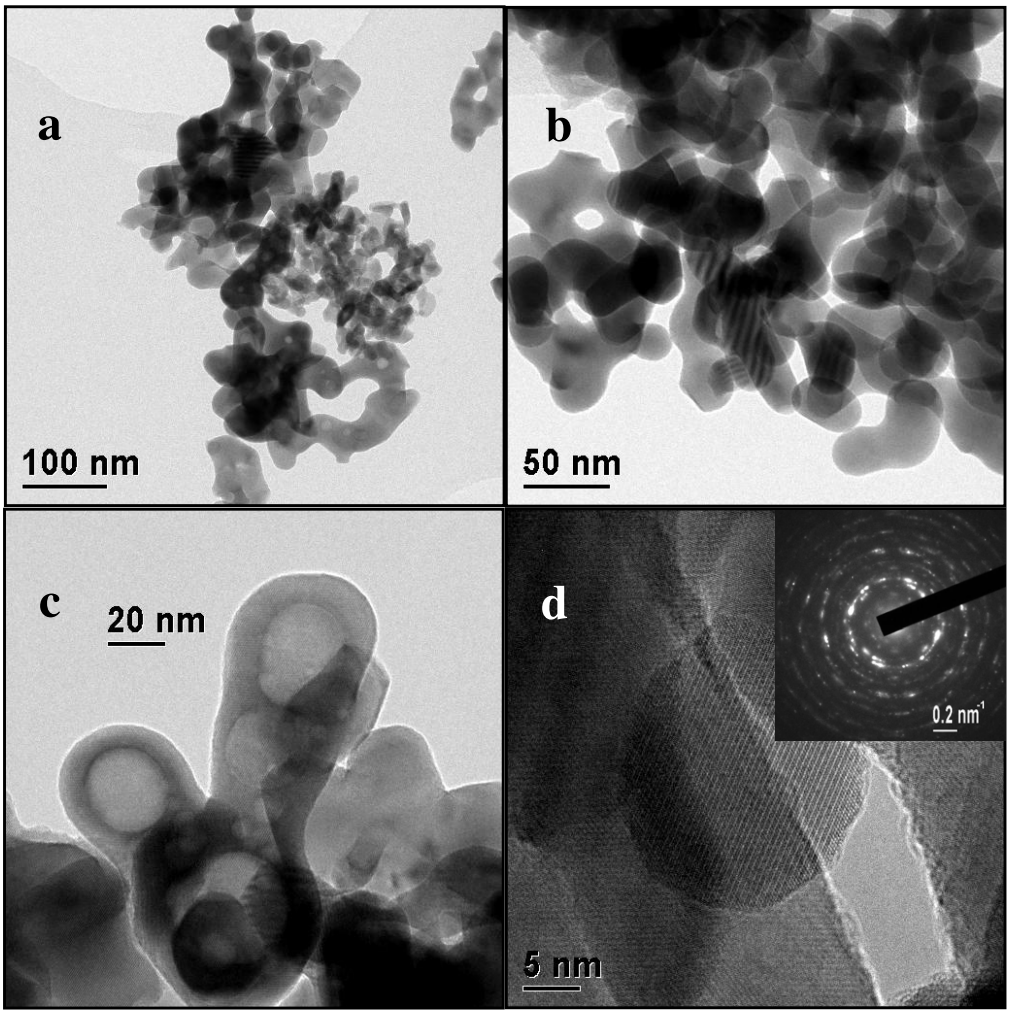

Figure 3. Transmission electron microscope (TEM) images and corresponding electron diffraction ring pattern of europium-doped LuGG nanocrystalline powders.

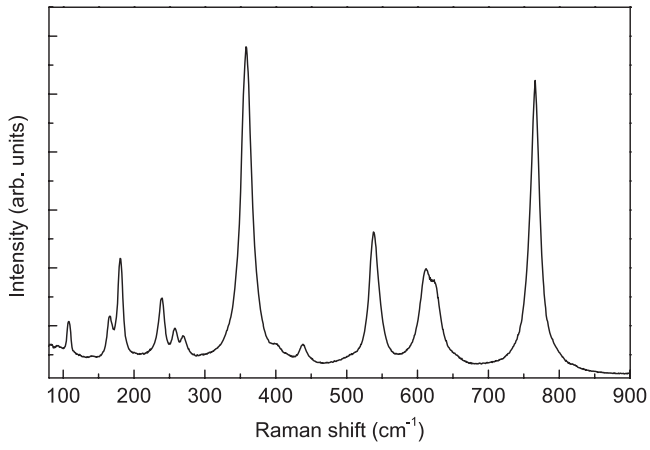

Figure 4. Room temperature Raman spectrum of nanocrystalline LuGG ($\lambda_{exc} = 488.0$ nm).

involving the whole tetrahedron. Finally, the bands below 380 cm^{-1} are due to O–Ga–O bending modes of the polyhedra and to lattice modes.

The diffuse reflectance infrared spectrum in the mid-infrared region for an undoped LuGG sample, shown in figure 5, indicates that impurities such as water and carbonate ions are present, shown by broad absorption bands around 3300 cm^{-1} and 1550 cm^{-1}, respectively. As a comparison, the diffuse reflectance spectra for GGG and YAG samples, prepared by the present Pechini technique (GGG) or by propellant synthesis (YAG), are presented. From this comparison, it can be noted the amount of carbonate ions and water is similar for these garnet hosts, even if the preparation procedure is vastly different. This behaviour suggests that the garnet hosts are not very hygroscopic. Besides, the Kubelka–Munk values of the absorption bands for the present garnets are notably lower than those observed for nanocrystalline Y_2O_3 prepared by a propellant technique [36], showing that the amount of these contaminants is much lower than found for sesquioxides. This behaviour agrees with the fact that sesquioxides are quite hygroscopic materials.

3.3. Luminescence properties

3.3.1. Eu^{3+} ion luminescence. Eu^{3+} is one of the most suitable luminescent lanthanide ion to be used as a structural probe because of its unique energy level structure with non-degenerate ground ($^7F_0$) and excited ($^5D_0$) states. Therefore,

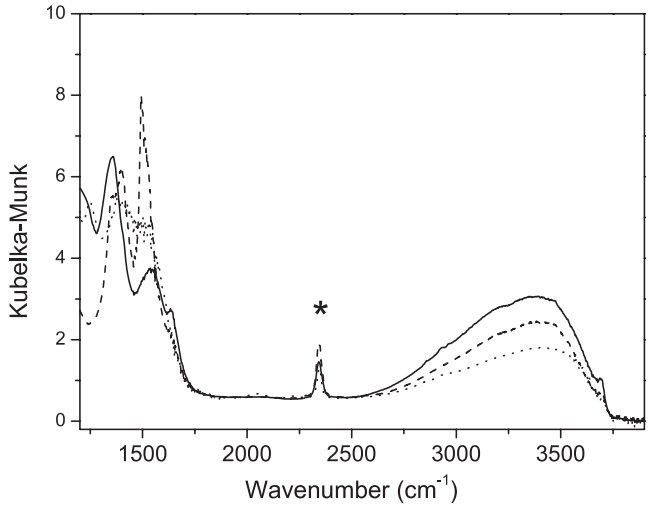

Figure 5. Infrared spectra in the mid-infrared region of nanocrystalline LuGG (solid line), GGG (dashed line) and YAG (dotted line). The star symbol denotes a band due to traces of carbon dioxide present in the FTIR spectrometer.

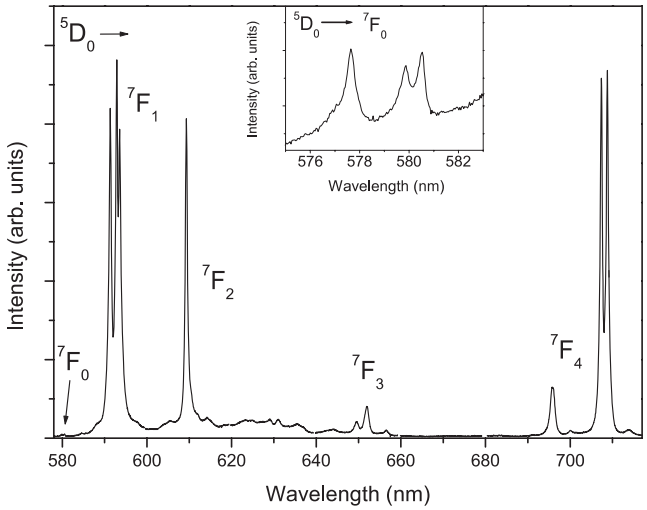

Figure 6. Room temperature luminescence spectrum of LuGG:Eu ($\lambda_{exc=395.0}$ nm). Inset: enlarged $D_0 \rightarrow {}^7F_0$ emission range.

the $^5D_0 \rightarrow {}^7F_0$ singlet to singlet transition is very useful to determine the number of different sites in which the Eu^{3+} ions are accommodated. Moreover, due to the fact that the $^5D_0$ excited state is a singlet, the number of the $^5D_0 \rightarrow {}^7F_J$ emission transitions depends on the splitting of the terminal ^7F_J level, which is in turn related to the local symmetry around the Eu^{3+} ion. The room temperature luminescence spectrum of the Eu^{3+}-doped LuGG sample in the visible range obtained upon 395 nm laser excitation is shown in figure 6. The spectrum consists of several bands assigned to $4f^6$–$4f^6$ transitions of the Eu^{3+} ion from the $^5D_0$ emitting level to the ^7F_J ($J = 0$–4) multiplets. From the spectra, the most intense emission bands are located at a wavelength around 590 nm and can be attributed to transitions between the $^5D_0$ and $^7F_1$ Stark levels. It is worth noting that the intensity of the magnetic dipole (MD) $^5D_0 \rightarrow {}^7F_1$ transition is independent of the local environment of the rare earth ion. On the other hand, the $^5D_0 \rightarrow {}^7F_2$ emission transition is electric dipole (ED) allowed and therefore its intensity is very sensitive to the Eu^{3+} ion environment.

Considering the ionic radii of the trivalent lanthanide ions, the dopant ions are expected to mainly substitute for the Lu^{3+} ions in dodecahedral sites. On the basis of the ED and MD selection rules, the number of expected emission bands for Eu^{3+} in D_2 symmetry is 0 and 3 for the $^5D_0 \rightarrow {}^7F_0$ and $^5D_0 \rightarrow {}^7F_1$ transitions, respectively [37]. The three strong bands peaked at wavelengths of 591.3, 592.9 and 593.6 nm can therefore be assigned to the Stark component of the $^5D_0 \rightarrow {}^7F_1$ transition, as in this case the degeneracy of the $J = 1$ multiplet is completely lifted in D_2 point symmetry [38]. Moreover, the bands in the 600–630 nm wavelength range can be assigned to ED-allowed $^5D_0 \rightarrow {}^7F_2$ transitions. The present attribution is also in agreement with the results obtained for an Eu^{3+}-doped YAG single crystal [39] and for nanocrystalline Eu^{3+}-doped YAG powders [40, 41]. Besides, the luminescence spectrum is similar to that observed for an Eu^{3+}-doped GGG garnet prepared with the same Pechini technique [42] while it is significantly different from those observed for Eu^{3+}-doped LuGG sample prepared by a sol–gel technique [26] as the relative intensities of the $^5D_0 \rightarrow {}^7F_1$ and $^5D_0 \rightarrow {}^7F_2$ emission bands appear to be different. We also note that the Eu^{3+} spectrum reported in [26] has a lower optical resolution with respect to the one obtained in the present work and therefore it is not possible to directly compare the energy positions of the bands of the emission spectra. The total energy splitting of the $^7F_1$ level can be evaluated from the peak energies of the $^5D_0 \rightarrow {}^7F_1$ transition bands. The energy difference between the highest and lowest component of the triplet is 64 cm^{-1}. This value is lower to that observed for an Eu^{3+}-doped YAG single crystal (about 200 cm^{-1} [39]) and also for a Eu^{3+} doped nanocrystalline GGG sample prepared by the Pechini method (about 160 cm^{-1} [43]). This behaviour indicates that the crystal field (CF) strength experienced by the Eu^{3+} ions is lower for the LuGG host than for YAG and GGG garnet hosts. A change of CF strength experienced by a lanthanide dopant ion on varying the Ga content on mixed Al–Ga yttrium garnets has been already observed for a Tb^{3+}-doped $Y_3(Al_xGa_{1-x})_5O_{12}$ sample. For this system, it was observed that the CF decreases monotonically on increasing the Ga percentage and assumes the lowest value for the $Y_3Ga_5O_{12}$ host [44]. This behaviour of the CF is attributed to a decrease of the partial charge on the oxygen ions and an increase of the lanthanide–oxygen distance on increasing the Ga percentage. The results found for the LuGG:Eu sample under investigation suggest, in agreement with those found for Tb^{3+}-doped yttrium Al–Ga garnets, that gallium-based garnets give rise to a lower crystal field experienced by lanthanide ions with respect to aluminium based garnets.

The ratio between the integrated intensity of the $^5D_0 \rightarrow {}^7F_2$ and that of the $^5D_0 \rightarrow {}^7F_1$ transitions

$$R = \frac{I(^5D_0 \rightarrow {}^7F_2)}{I(^5D_0 \rightarrow {}^7F_1)} \quad (1)$$

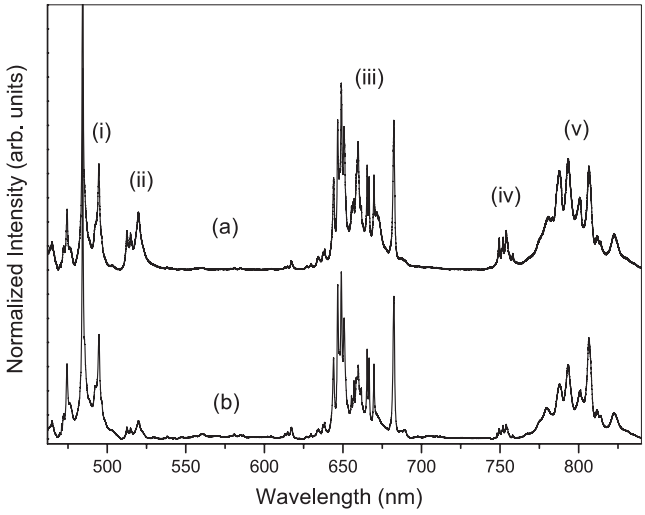

Figure 7. Room temperature luminescence spectra of LuGG:Tm ($\lambda_{exc} = 454.6$ nm) at a laser power of 10 mW (a) and 20 mW (b). (i) $^1G_4 \rightarrow {}^3H_6$, (ii) $^1D_2 \rightarrow {}^3H_5$, (iii) $^1G_4 \rightarrow {}^3F_4$, $^1D_2 \rightarrow {}^3H_4$, (iv) $^1D_2 \rightarrow {}^3F_3$, (v) $^1G_4 \rightarrow {}^3H_5$, $^1D_2 \rightarrow {}^3F_2$, $^3H_4 \rightarrow {}^3H_6$.

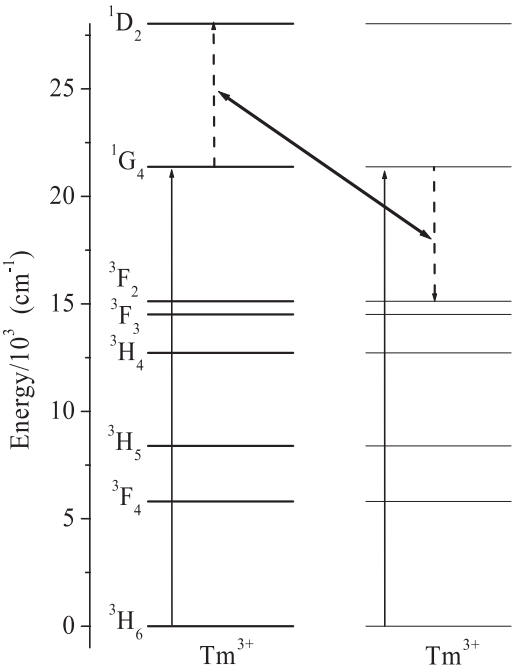

Figure 8. Schematic representation of the ETU process populating the $^1D_2$ level of Tm^{3+} upon excitation at 454.5 nm.

can be considered as indicative of the asymmetry of the coordination polyhedron around the Eu^{3+} ion [45]. The value of the asymmetry ratio can be estimated from the emission spectrum and results to be around 1.0. This value is much lower than that found for nanocrystalline GGG samples prepared by coprecipitation (4.8), Pechini (3.1) and combustion synthesis (1.5) [42], indicating that the coordination sphere of the Eu^{3+} ions is less distorted for the LuGG nanocrystalline samples under investigation. Moreover, the relatively low value of the asymmetry ratio R suggests that the Eu^{3+} ions are, on average, accommodated in a quite symmetric environment [46]. It is well known that the Eu^{3+} ion is a powerful structural probe to show the presence of different sites accommodating the lanthanide ions in the lattice. Particularly meaningful are the Eu^{3+} emission bands in the emission range around 580 nm, since they are due to $^5D_0 \rightarrow F_0$ singlet-to-singlet transitions. The emission spectrum in this region is shown in the inset of figure 6. Three weak emission bands at 577.6, 579.8 and 580.5 nm due to $^5D_0 \rightarrow {}^7F_0$ transitions are observed, indicating the presence of at least four minor sites for the Eu^{3+} ions. In fact, as mentioned before, the $^5D_0 \rightarrow {}^7F_0$ transition should not be observed for an Eu^{3+} ion accommodated in a D_2 point symmetry, since it is forbidden for this symmetry. On the other hand, it has been shown in the literature that other garnets, such as YAG or GGG, can have other possible incorporation mechanisms [47–49]. The observed $^5D_0 \rightarrow {}^7F_0$ transitions indicate the presence of several non-regular garnet sites occupied by the Eu^{3+} ions.

The luminescence decay curve for the Eu^{3+}-doped sample (not shown) exhibits a non-exponential behaviour. Hence, the average lifetime can be evaluated by using the following equation:

$$\tau_{avg} = \frac{\int t I(t)\,dt}{\int I(t)\,dt}. \quad (2)$$

The average lifetime (τ_{avg}) of the $^5D_0$ level is found to be 3.31 ms which is comparable to the one observed for Eu^{3+} ions in GGG prepared by propellant (3.3 ms) and Pechini (3.1 ms) synthesis [42]. The non-exponential nature of the decay curve can be due to the presence of different sites for the Eu^{3+} ions.

3.3.2. Tm^{3+} ion luminescence. The room temperature luminescence spectrum of the Tm^{3+}-doped LuGG sample, shown in figure 7, was obtained upon 454.6 nm laser excitation, which directly populates the $^1G_4$ excited level of the Tm^{3+} ion. The spectrum shows a blue-green emission around 485 nm, which can be assigned to the $^1G_4 \rightarrow {}^3H_6$ transition. The red emission around 650 nm is due to the $^1G_4 \rightarrow {}^3F_4$ and $^1D_2 \rightarrow {}^3H_4$ transitions (see below). Interestingly, some bands around 520 and 750 nm are present in the spectrum, which are not observed in the emission spectrum of a Tm^{3+}-doped GGG nanocrystalline sample prepared by the same technique [50]. Moreover, the intensity of these bands, normalizing the spectrum to the $^1G_4 \rightarrow {}^3H_6$ emission band, increases on increasing the laser power, as shown in figure 7. On the basis of the energy level scheme of Tm^{3+} in garnets [51], these emission bands can be straightforwardly attributed to transitions starting from the $^1D_2$ level. It is worth noting that in the present case the laser exciting power density on the sample is relatively high, due to the employed experimental set-up, as the laser beam is highly focused on the sample, using a microscopy objective. Since the intensity of these bands depends nonlinearly on the laser power, an energy transfer upconversion (ETU) mechanism is most probably present, involving two photons that can populate the $^1D_2$ level (see figure 8). In fact, the energy difference between the $^1D_2$ and $^1G_4$ levels (about 6600 cm^{-1}) is very similar to the one between the $^1G_4$ and the next lower lying $^3F_2$ level (6250 cm^{-1}). Therefore, two ions that have been excited to

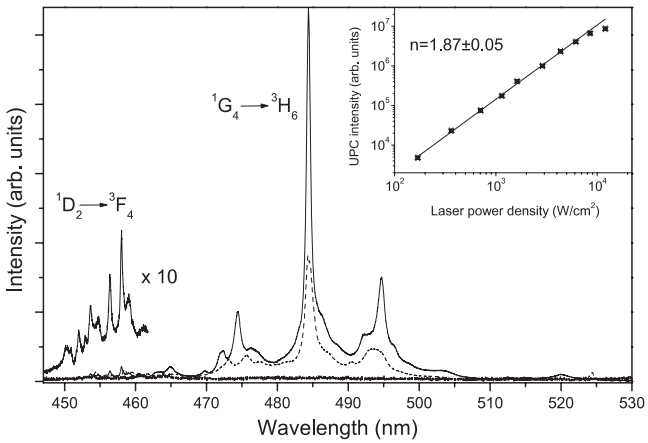

Figure 9. Upconversion spectra for LuGG:Tm (solid line), GGG:Tm (dashed line) and Y_2O_3:Tm (dotted line) nanocrystalline samples ($\lambda_{exc} = 645.7$ nm). Inset: power study ($\lambda_{em} = 485$ nm).

the $^1G_4$ level, upon excitation at 454.6 nm, can undergo a ($^1G_4$, $^1G_4$) $\rightarrow$ ($^1D_2$, $^3F_2$) energy transfer, which requires the absorption of low energy phonons of about 350 cm^{-1}, which are present in the nanocrystalline host, as shown from the Raman spectrum (see figure 4 and table 2). Subsequently, the ions in the $^1D_2$ level can radiatively decay to lower lying levels. In fact, on the basis of the Tm^{3+} energy levels in garnets, the bands around 520 and 755 nm can be attributed to $^1D_2 \rightarrow {}^3H_5$ and $^1D_2 \rightarrow {}^3F_3$ transitions, respectively [51]. The bands observed in the near-infrared around 800 nm are attributed to the $^1G_4 \rightarrow {}^3H_5$, $^3H_4 \rightarrow {}^3H_6$ and also $^1D_2 \rightarrow {}^3$ F2 transitions, which give rise to overlapping emissions.

Upon excitation at 645.7 nm, which directly populates the $^3F_2$ level of the Tm^{3+} ion, a strong upconversion emission in the blue-green region (450–500 nm) is observed (see figure 9). Bands attributed to both the $^1D_2 \rightarrow {}^3F_4$ and $^1G_4 \rightarrow {}^3H_6$ transitions are present, even if the emission due to the $^1G_4 \rightarrow {}^3H_6$ transition is much stronger than that due to the $^1D_2 \rightarrow {}^3F_4$ one. The upconversion intensity I_{UPC} is related to the laser power density P by the equation $I_{UPC} \propto P^n$, where n is the number of photons involved in the upconversion process. Therefore, from a power study, in which the upconversion intensity is monitored as a function of the laser power density, the n value can be determined.

The fit of the logarithm of I_{UPC} versus the logarithm of P gives an n value of 1.87 ± 0.05 (see the inset of figure 9), indicating that two photons are involved in the upconversion process. From the figure, it is also worth noting that, for a power density higher than 8×10^3 W cm^{-2}, the upconversion intensity is starting to deviate from a quadratic power law and a saturation behaviour starts to take place. In figure 10 a schematic representation of the expected upconversion processes populating the $^1G_4$ and $^1D_2$ levels of the Tm^{3+} ions upon excitation at 645.7 nm is proposed. First, one pump photon excites the Tm^{3+} ions to the $^3F_2$ level. After that, the Tm^{3+} ion relaxes non-radiatively to the $^3H_4$ level and then another photon (or an energy transfer from a neighbouring Tm^{3+} ion) can excite the ion to the $^1D_2$ level. Then, the Tm^{3+} ions can radiatively decay to the $^3F_4$ level and blue emission is observed. On the other hand, the Tm^{3+} ion excited in the $^3H_4$ level can further non-radiatively decay to the $^3F_4$ level and then a pump photon (or an energy transfer from another Tm^{3+} ion) can excite the ion to the $^1G_4$ level, from which the $^1G_4 \rightarrow {}^3H_6$ transition is originated. It is also important to remark that few investigations have been carried out on these upconversion processes. Upconversion emission upon red excitation at 656 nm was observed for Tm^{3+}-doped nanocrystalline Y_2O_3 by Vetrone *et al* [52]. An upconversion emission in the 470–510 region was also observed for a Tm^{3+}-doped ZrO_2 nanocrystalline sample, upon excitation at 649 nm [53]. For the sake of comparison with other Tm^{3+}-doped nanocrystalline garnets, we measured the upconversion emission in the same experimental conditions (such as pump power and measurement geometry) for Tm^{3+} doped nanocrystalline GGG prepared with the same sol–gel citric acid procedure [54]. We point out that the average particle size and morphology of the present LuGG and GGG samples are very similar, as evidenced in previous papers [43, 54]. In particular, the average particle size for nanocrystalline GGG is around 50 nm. The comparison between the two emissions of the Tm^{3+}-doped garnet hosts, measured in the same experimental conditions, is shown in figure 9. It is evident that the LuGG host shows significantly stronger upconversion emission (about 2:1 integrated intensity ratio) with respect to the GGG sample. As a further comparison, a freshly prepared Tm^{3+}-doped nanocrystalline Y_2O_3 sample using a propellant synthesis, as reported by Polizzi *et al* [55], shows a very weak upconversion emission, which is practically negligible with respect to that observed for the LuGG and GGG doped samples (see figure 9). Although the particle size and morphology for nanocrystalline Y_2O_3 (average size in the 20–50 nm range [54]) is similar than for GGG and LuGG samples, it should be noted that the amount of contaminants such as carbonates and water is much higher in the Y_2O_3 sample. Therefore, a higher non-radiative de-excitation probability and therefore a lower emission intensity is expected for the Y_2O_3 sample with respect to the GGG and LuGG ones, in agreement with the present experimental results. This behaviour points to a possible use of lanthanide-doped LuGG as a material in an efficient upconversion phosphor which can be efficiently pumped by relatively cheap diode lasers in the red region.

Upon excitation with the third harmonic radiation of the Nd:YAG laser (355 nm), the Tm^{3+}-doped LuGG sample shows strong emission bands in the 450–460 nm region (as shown in figure 9), assigned to $^1D_2 \rightarrow {}^3F_4$ transition. The RT luminescence decay curve of this transition, monitored at a wavelength of 459 nm (not shown), has a non-exponential behaviour. The non-exponential nature of the decay can be explained considering the presence of different sites for the Tm^{3+} ions, as shown for the Eu^{3+}-doped sample, and also of cross-relaxation processes between neighbouring Tm^{3+} ions, as described above. This is not unusual for the present Tm^{3+} concentration, as described for Tm^{3+}-doped GGG [6]. The effective decay time of the $^1D_2$ level, obtained from equation (2), results to be 37.2 μs. This value is similar to that found for a Tm^{3+}-doped GGG nanocrystalline sample prepared by a combustion procedure [6].

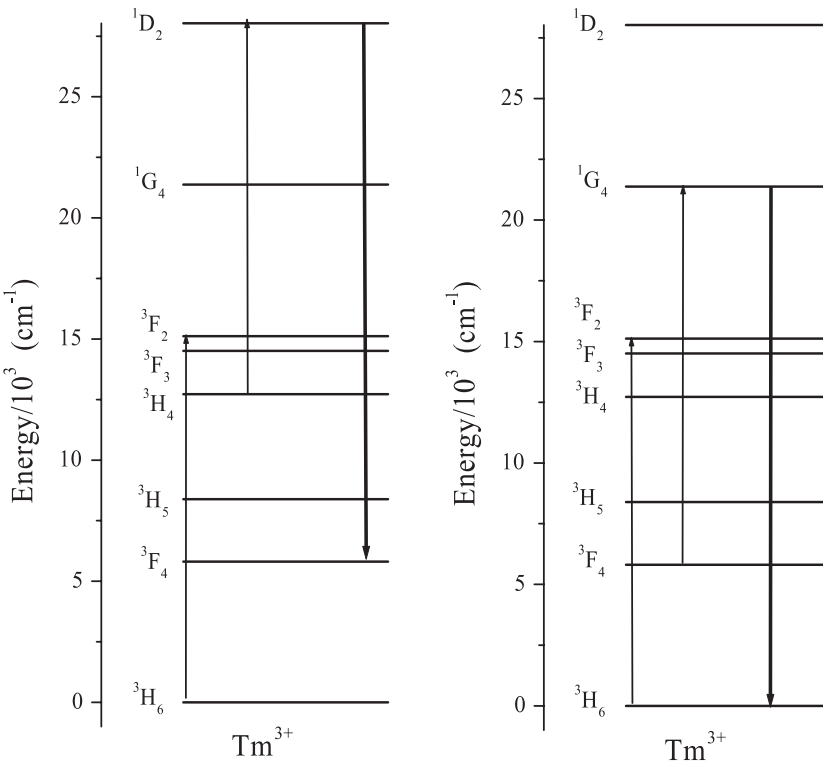

Figure 10. Schematic representation of excited state absorption upconversion processes for Tm^{3+} ions upon excitation at 645.7 nm.

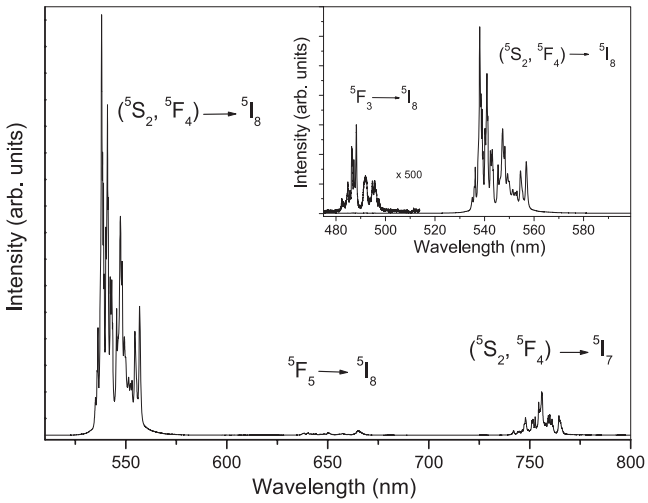

Figure 11. Room temperature luminescence spectrum of LuGG:Ho ($\lambda_{exc} = 454.5$ nm). Inset: upconversion spectrum for LuGG:Ho ($\lambda_{exc} = 645.7$ nm).

3.3.3. Ho^{3+} ion luminescence. Upon 457.5 nm excitation, emission bands due to 4f–4f transitions of Ho^{3+} ions are observed, as shown in figure 11. A dominant green emission around 550 nm can be assigned to transitions from the ($^5F_4$, $^5S_2$) thermalized levels to the $^5I_8$ ground state. A much weaker emission is observed in the red region around 650 nm, due to the $^5F_5 \rightarrow {}^5I_8$ transition. A near-infrared emission between 730 and 780 nm is also observed, corresponding to the ($^5F_4$, $^5S_2$) $\rightarrow {}^5I_7$ transition. A very weak, but detectable, emission is also observed in the 480–500 nm region, which can be assigned to the $^5F_3 \rightarrow {}^5I_8$ transition. The emission spectrum is similar to that observed for a Ho^{3+}-doped nanocrystalline GGG sample prepared by a propellant synthesis [56]. We found it interesting to compare the emission intensity of the present LuGG sample with other Ho^{3+}-doped nanocrystalline common oxide hosts, under the same experimental conditions, as laser pump wavelength (457.5 nm), laser power and measurement set-up. The hosts that have been considered are Y_2O_3, YAG and GGG, doped with 1% of Ho^{3+} with respect to Y^{3+} (for Y_2O_3 and YAG samples) or Gd^{3+} (for GGG sample). The Y_2O_3 sample has been freshly prepared with a propellant synthesis [55], while the YAG and GGG samples have been prepared with a propellant technique [42] and a citric acid sol–gel procedure [54], respectively. The details on the particle size and morphology of the YAG samples prepared by a combustion procedure has been reported by Krsmanovic *et al* [57]. In particular, electron microscopy images show that the nanoparticles have a broad size distribution with an average particle size around 50 nm. Moreover, TEM images show that at the nanometric scale the particles have a round shape and are notably aggregated, as found for Y_2O_3 and the GGG and LuGG garnet samples under investigation [43, 54, 55]. Figure 12 shows the comparison of the emission spectra and the integrated intensity in the visible region for the different hosts (in the figure inset). It turns out evidently that the LuGG sample shows the highest integrated intensity. To our knowledge, this is the first direct experimental evidence of an increase of the luminescence emission in Ho^{3+}-doped garnet hosts in which the Y^{3+} ion has been substituted by the Lu^{3+} ion. An increase of the luminescence emission

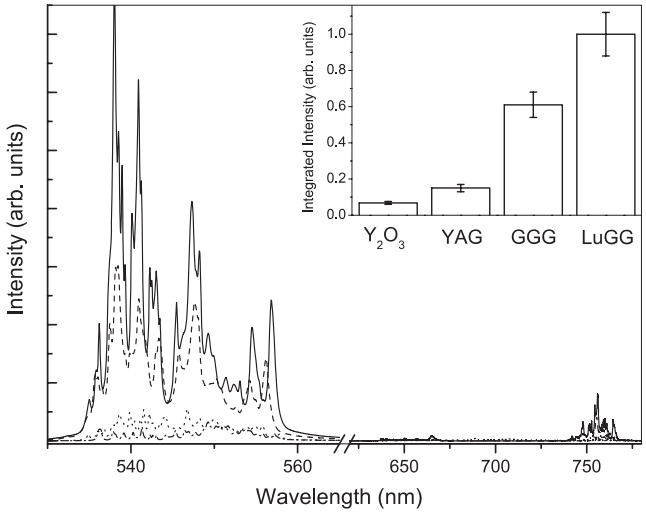

Figure 12. Room temperature luminescence spectra ($\lambda_{exc} = 454.5$ nm) for LuGG:Ho (solid line), GGG:Ho (dashed line), YAG:Ho (dotted line) and Y_2O_3:Ho (dashed–dotted line) nanocrystalline samples (YAG:Ho and Y_2O_3:Ho samples are prepared by a propellant synthesis [51]). Inset: comparison of the integrated intensities.

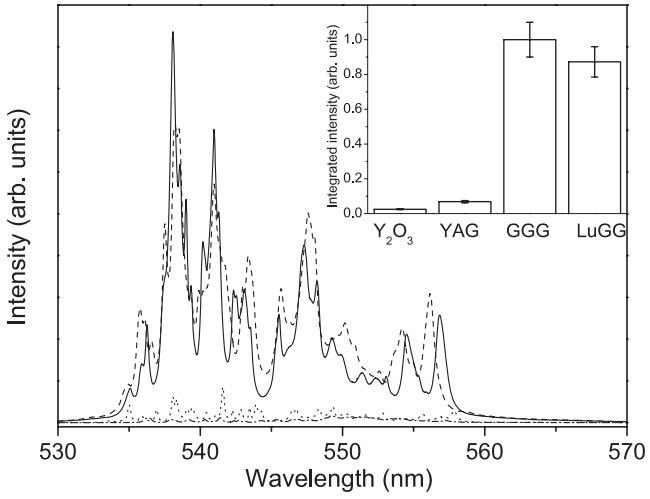

Figure 13. Room temperature upconversion spectra ($\lambda_{exc} = 645.7$ nm) for LuGG:Ho (solid line), GGG:Ho (dashed line), YAG:Ho (dotted line) and Y_2O_3:Ho (dashed–dotted line) nanocrystalline samples (YAG:Ho and Y_2O_3:Ho samples are prepared by a propellant synthesis [51]). Inset: comparison of the integrated intensities.

intensity of Nd^{3+} ions in vanadate hosts due to the substitution of yttrium with lutetium was also observed by Maunier *et al* [20]. In particular, in this investigation, a Nd^{3+}-doped $LuVO_4$ single crystal shows a higher emission cross section in the infrared region with respect to Nd^{3+} doped YVO_4 and $GdVO_4$ samples. This behaviour was attributed to an intensity-borrowing mechanism that mixes the 4f and 5d rare earths orbitals through lattice valence band energy levels. This mechanism could be enhanced because of an increasing hybridization of the emitting lanthanide ion and Lu^{3+} 4f orbitals. We also note that no investigation has been reported in the literature on the Judd–Ofelt parameters for the Ho^{3+} ion in the LuGG host. The emission decay curve, upon excitation at 355 nm and monitored at 530 nm, shows mainly an exponential behaviour, suggesting that the lanthanide ions have on average similar environments and/or there is no strong energy transfer between neighbouring ions. The room temperature measured decay time of the ($^5F_4$, $^5S_2$) thermalized levels is 37.6 μs. Unfortunately, no radiative lifetimes of Ho^{3+} excited states nor Judd–Ofelt intensity parameters for LuGG:Ho are available in the literature and therefore it is not possible to estimate the luminescence efficiency of the green transition. On the other hand, this value is similar to that found for the same transition at room temperature for a Ho^{3+} doped GGG nanocrystalline sample (49 μs) [56].

Upconversion spectra for the LuGG:Ho sample and other 1% Ho^{3+}-doped oxide hosts upon excitation at 647 nm are shown in figure 11 (inset) and in figure 13. A green emission, around 540 nm, due to the ($^5F_4$, $^5S_2$) $\rightarrow$ $^5I_8$ transition is observed. Moreover, a weak but detectable emission is visible in the 480–500 nm region, due to the $^5F_3 \rightarrow {}^5I_8$ transition. A comparison of the integrated upconversion intensities in the 530–560 nm region (shown in the inset of figure 13) for different hosts clearly indicates that the Ho^{3+}-doped LuGG host has one of the highest values, very close

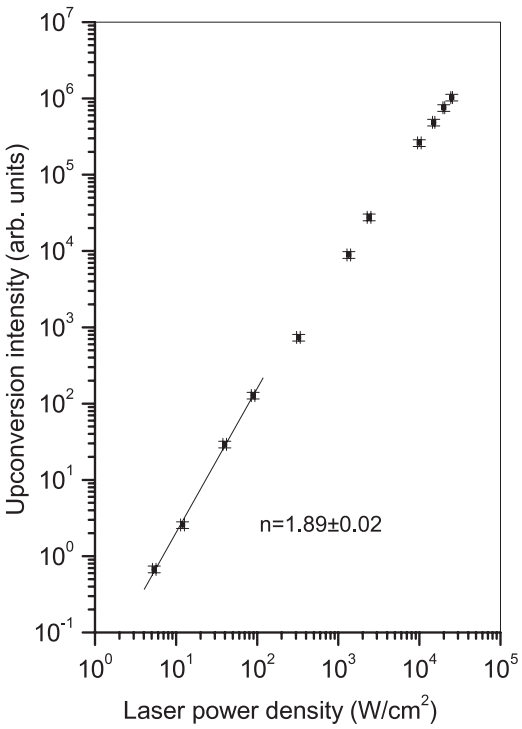

Figure 14. Power study for the LuGG:Ho sample ($\lambda_{exc} = 645.7$ nm, $\lambda_{em} = 485$ nm).

to that obtained for the Ho^{3+}-doped GGG sample, about one order of magnitude higher with respect to the YAG sample. Besides, a very careful power study of the green emission has been carried out, in order to determine the number of photons involved in the upconversion process. The slope of the fit of the logarithm of the upconversion intensity versus the logarithm of the power density is 1.89 ± 0.02 (see figure 14), indicating the occurrence of a two-photon mechanism, as found for an Ho^{3+}-

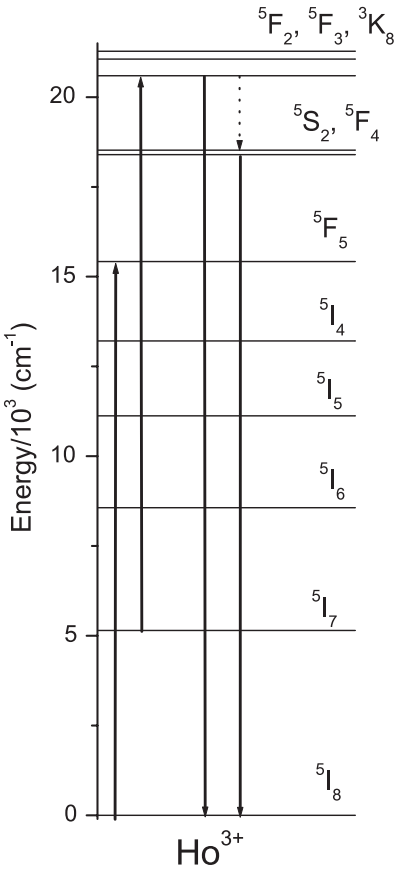

Figure 15. Schematic representation of the excited state absorption upconversion processes for Ho^{3+} ions upon excitation at 645.7 nm.

doped nanocrystalline GGG [56]. From the power plot it is clear that, for power density higher than 8×10^3 W cm^{-2}, the upconversion intensity is starting to deviate from a quadratic power law and a saturation behaviour starts to become evident. An excited state absorption (ESA) is most probably the most efficient upconversion mechanism [56], as illustrated in the following. After the absorption of a photon at 647 nm, the $^5F_5$ level is initially populated which then decays through non-radiative processes to the $^5I_7$ level (figure 15). Then, a second absorbed photon can bring the Ho^{3+} ion to the $^5F_3$ level, which can undergo a radiative decay, giving rise to the blue emission (480–500 nm, see the inset of figure 11). The $^5F_3$ level can also non-radiatively decay to the lower lying ($^5F_4$, $^5S_2$) thermalized levels, and in turn a radiative transition to the ground state occurs, giving rise to the stronger green emission, in the 535–560 nm region. It is worth pointing out that the green upconversion emission is clearly evident even for laser power density as low as 4 W cm^{-2}, an aspect that makes this material strongly interesting for its use as an upconversion phosphor in the green region upon excitation in the red.

4. Conclusions

Nanocrystalline $Lu_3Ga_5O_{12}$ samples doped with 1.0 mol% of trivalent lanthanide ions (Pr^{3+}, Eu^{3+}, Gd^{3+}, Ho^{3+}, Er^{3+} and Tm^{3+}) were prepared via a citric acid sol–gel process. A Rietveld analysis of the x-ray powder pattern and a Raman characterization revealed that all the samples are single-phase cubic garnet. The lanthanide ions are incorporated in the garnet lattice structure, substituting for the Lu^{3+} ions, as the lattice constant increases on increasing the lanthanide ion size, according to Végard's law. An apparent large lattice constant has been obtained for the europium-doped sample, suggesting the presence of Eu^{2+} ions generated during the x-ray irradiation process and quickly converted to Eu^{3+} ions by an ion–hole recombination process.

Electron microscopy images show that the nanoparticles have an average size of 40 nm, which is consistent with the results obtained from the Rietveld analysis.

The emission spectrum for the Eu^{3+}-doped sample shows typical bands due to $^5D_0 \rightarrow {}^7F_J$ ($J = 0, 1, 2, 3, 4$) transitions. The broadening of these emission bands and the non-exponential behaviour of the decay curve indicate the presence of structural disorder around the lanthanide ions.

Investigation of the emission of Tm^{3+}- and Ho^{3+}-doped nanocrystalline LuGG proved that these materials have interesting luminescence properties compared to other doped nanocrystalline oxide hosts, such as $Gd_3Ga_5O_{12}$, $Y_3Ga_5O_{12}$ and Y_2O_3. The intensity of the upconversion emission in the blue-green regions for the Tm^{3+}- and Ho^{3+}-doped samples shows a significant increase upon 647.5 nm excitation with respect to GGG, YAG and Y_2O_3 hosts doped with the same lanthanide ions. In particular, the green upconversion emission of the LuGG:Ho sample is clearly visible for laser power density as low as 4 W cm^{-2}, which makes this material strongly interesting for its use as an upconversion phosphor in the green region upon excitation in the red.

Acknowledgments

The authors thank Erica Viviani (Università di Verona) for expert technical help. The financial support of the Fondazione Cariverona, under contract with the University of Verona, is gratefully acknowledged. Finally, the authors acknowledge the MIUR of Italy for financial support under MOU between the University of Verona and Department of Physics, S V University, Tirupati, India.

References

[1] Boyer J C, Cuccia L A and Capobianco J A 2007 *Nano Lett.* **7** 847
[2] Li L, Jiang W G, Pan H H, Xu X R, Tang Y X, Ming J Z, Xu Z D and Tang R K 2007 *J. Phys. Chem.* C **111** 4111
[3] Diamente P R, Raudsepp M and van Veggel F C J M 2007 *Adv. Funct. Mater.* **17** 363
[4] Ferreira R A S, Karmaoui M, Nobre S S, Carlos L D and Pinna N 2006 *ChemPhysChem* **7** 2215
[5] Li L, Tsung C-K, Yang Z, Stucky G D, Sun L D, Wang J F and Yan C H 2008 *Adv. Mater.* 903
[6] Krsmanovic R, Morozov V A, Lebedev O I, Polizzi S, Speghini A, Bettinelli M and Van Tendeloo G 2007 *Nanotechnology* **18** 325604
[7] Naccache R, Vetrone F, Boyer J C, Capobianco J A, Speghini A and Bettinelli M 2004 *J. Nanosci. Nanotechnol.* **4** 1025

[8] Setlur A A and Srivastava A M 2007 *Opt. Mater.* **29** 1647
[9] Chénais S, Druon F, Balembois F, Georges P, Brenier A and Boulon G 2003 *Opt. Mater.* **22** 99
[10] Kir'yanov A V, Aboites V, Belovolov A M, Timoshechkin M I, Belovolov M I, Damzen M J and Minassian A 2002 *Opt. Express* **10** 832
[11] Grinberg M, Kuklinski B, Wisniewski K, Koepke C, Lukasiewicz T, Kisielewski J, Swirkowicz M and Suchocki A 2003 *J. Opt. Soc. Am.* B **20** 577
[12] Doug J, Ueda K I and Kaminskii A A 2007 *Opt. Lett.* **32** 3266
[13] Li H L, Liu X J and Huang L P 2005 *J. Am. Ceram. Soc.* **88** 3226
[14] Nikl M, Pejchal J, Mihokova E, Mares J A, Ogino H, Yoshikawa A, Fukuda T, Vedda A and D'Ambrosio C 2006 *Appl. Phys. Lett.* **88** 141916
[15] Ozen G and DiBartolo B 1999 *Appl. Spectrosc.* **53** 1454
[16] Ogino H, Yoshikawa A, Lee J H, Nikl M, Solovieva N and Fukuda T 2004 *Radiat. Meas.* **38** 485
[17] Nikl M, Vedda A, Fasoli M, Fontana I, Laguta V V, Mihokova E, Pejchal J, Rosa J and Nejezchleb K 2007 *Phys. Rev.* B **76** 195121
[18] Tondelli A, Alshourbagy M and Tonelli M 2008 *J. Appl. Phys.* **104** 104916
[19] Spangler L H, Farris B, Filer E D and Bames N P 1996 *J. Appl. Phys.* **79** 573
[20] Maunier C, Doualan J L, Moncorgé R, Speghini A, Bettinelli M and Cavalli E 2002 *J. Opt. Soc.* B **19** 1794
[21] Speghini A, Piccinelli F and Bettinelli M 2010 *Modern Aspects of the Luminescence of Rare-Earth doped Materials* ed R Mahiou and P Boutinaud (Kerala, India: Transworld Research Network)
[22] Hreniak D, Strek W, Gluchowski P, Bettinelli M and Speghini A 2008 *Appl. Phys.* B **91** 89
[23] Caponetti E, Martino D C, Saladino M L and Leonelli C 2007 *Langmuir* **23** 3947
[24] Naccache R, Vetrone F, Speghini A, Bettinelli M and Capobianco J A 2008 *J. Phys. Chem.* C **112** 7750
[25] Venkatramu V, Falcomer D, Speghini A, Bettinelli M and Jayasankar C K 2008 *J. Lumin.* **128** 811
[26] Liu X, Zhu L, Wang L, Yu C and Lin J 2008 *J. Electrochem. Soc.* **155** P21
[27] Young R A (ed) 1993 *The Rietveld Method* (Oxford: University Press)
[28] Lutterotti L and Gialanella S 1998 *Acta Mater.* **46** 101
[29] Euler F and Bruce J A 1965 *Acta Crystallogr.* **19** 971
[30] www.webelements.com
[31] Mihokova E, Vedda A, Fasoli M, Moretti F, Bulin A-L, Nikl M, Bettinelli M, Speghini A, Ogino H and Yoshikawa A, submitted
[32] Hurrell J P, Porto S P S, Chang I F, Mitra S S and Bauman R P 1958 *Phys. Rev.* **173** 851
[33] Song J J, Klein P B, Wadsack R L, Selders M, Mroczkowski S and Chang R K 1973 *J. Opt. Soc. Am.* **63** 1135
[34] Saine M C, Husson E and Brusset H 1982 *Spectrochim. Acta* A **38** 25
[35] Cavalli E, Zannoni E, Bettinelli M, Speghini A, Tonelli M and Tondelli A 2000 *J. Phys.: Condens. Matter* **12** 4665
[36] Vetrone F, Boyer J-C, Capobianco J A, Speghini A and Bettinelli M 2003 *J. Phys. Chem.* B **107** 10747
[37] Gross H, Neukum J, Heber J, Mateika D and Xiao T 1993 *Phys. Rev.* B **48** 9264
[38] Kaminskii A A 1990 *Laser Crystals* (Berlin: Springer)
[39] Shen Y, Li C, Costa V C and Bray K L 2003 *Phys. Rev.* B **68** 014101
[40] Potdevin A, Chadeyron G, Boyer D, Caillier B and Mahiou R 2005 *J. Phys. D: Appl. Phys.* **38** 3251
[41] Hreniak D, Holsa J, Lastusaari M and Strek W 2007 *J. Lumin.* **122** 91
[42] Daldosso M, Falcomer D, Speghini A, Ghigna P and Bettinelli M 2008 *Opt. Mater.* **30** 1162
[43] Martin-Rodriguez R, Valiente R, Polizzi S, Bettinelli M, Speghini A and Piccinelli F 2009 *J. Phys. Chem.* C **113** 12195
[44] Mayolet A, Zhang W, Simoni E, Krupka J C and Martin P 1995 *Opt. Mater.* **4** 757
[45] Oomen E W J L and van Dongen A M A 1989 *J. Non-Cryst. Solids* **111** 205
[46] Reisfeld R, Zigansky E and Gaft M 2004 *Mol. Phys.* **102** 1319
[47] Maglia F, Buscaglia V, Gennari S, Ghigna P, Dapiaggi M, Speghini A and Bettinelli M 2006 *J. Phys. Chem.* B **110** 6561
[48] Lupei V 2002 *Opt. Mater.* **19** 95
[49] Lupei V, Lupei A and Boulon G 1994 *J. Physique* IV **C4** 407
[50] Pandozzi F, Vetrone F, Boyer J-C, Naccache R, Capobianco J A, Speghini A and Bettinelli M 2005 *J. Phys. Chem.* B **109** 17400
[51] Lupei A, Lupei V, Grecu S, Tiseanu C and Boulon G 1994 *J. Appl. Phys.* **75** 4652
[52] Vetrone F, Boyer J-C, Capobianco J A, Speghini A and Bettinelli M 2004 *Nanotechnology* **15** 75
[53] Patra A, Ghosh P, Chowdhury P S, Alencar M A R C, Lozano B W, Rakov N and Maciel G S 2005 *J. Phys. Chem.* B **109** 10142
[54] Dal Dosso M, Falcomer D, Speghini A, Bettinelli M, Enzo S, Lasio B and Polizzi S 2008 *J. Alloys Compounds* **451** 553
[55] Polizzi S, Fagherazzi G, Battaglin G, Bettinelli M and Speghini A 2001 *J. Mater. Res.* **16** 146
[56] Boyer J-C, Vetrone F, Capobianco J A, Speghini A, Zambelli M and Bettinelli M 2004 *J. Lumin.* **106** 263
[57] Krsmanovic R, Canton P, Speghini A, Bettinelli M and Polizzi S 2004 *Prog. Adv. Mater. Processes, Mater. Sci. Forum* **453/454** 251